

## Supporting information

# Reactivation of Sulfide-Protected [FeFe] Hydrogenase in a Redox-active Hydrogel

Alaa A. Oughli<sup>a\*</sup>, Steffen Hardt<sup>a</sup>, Olaf Rüdiger<sup>b</sup>, James A. Birrell<sup>b\*</sup> and Nicolas Plumeré<sup>a\*</sup>

---

<sup>a</sup>Centre for Electrochemical Sciences—Molecular Nanostructures, Ruhr-Universität Bochum Universitätsstrasse 150, 44780 Bochum (Germany). E-Mail: nicolas.plumere@rub.de; alaa.alsheikhoughli@rub.de

<sup>b</sup>Max Planck Institute for Chemical Energy Conversion, Stiftstrasse 34–36, 45470 Mülheim an der Ruhr (Germany). E-Mail: james.birrell@cec.mpg.de

## **1. Methods**

### **1.1 Polymer synthesis**

The synthesis of the viologen modified polymer P1 (Scheme S1) was carried out according to ref [1].

### **1.2 DdHydAB sample preparation**

DdHydAB was prepared heterologously in *E. coli* BL21(DE3)  $\Delta$ iscR cells, purified by Strep-tag affinity chromatography, and artificially matured with diiron precursor complex as described previously.<sup>2</sup> The sulfide-protected enzyme was generated by oxidizing the active enzyme with hexaammine-ruthenium (III) chloride under an N<sub>2</sub> atmosphere, in the presence of Na<sub>2</sub>S, as described previously.<sup>3</sup>

### **1.3 Electrode preparation**

Prior to electrode drop-casting, glassy carbon working electrode (GCE) was polished with 1, 0.3 and 0.05  $\mu$ m Al<sub>2</sub>O<sub>3</sub> slurry then rinsed with ultrapure water and sonicated in water for 10 min. For the preparation of P1/DdHydAB redox hydrogel, a solution of DdHydAB (1  $\mu$ L, 200  $\mu$ M in 50 mM Tris-HCl buffer, pH 8) was mixed with an aqueous solution of P1 (5  $\mu$ L, 6 mg mL<sup>-1</sup>). The mixture was drop-cast on a GCE and left to dry at 4 °C for 16 h. For DET measurements, a pyrolytic graphite electrode was polished with sand paper (P280) then with alumina paste (1  $\mu$ m grain size) in the glovebox. Afterwards, DdHydAB (5  $\mu$ L, 50  $\mu$ M in 50 mM Tris-HCl buffer, pH 8) was placed on the electrode surface and left for 10 min. The electrode was then rinsed with water and placed in the electrochemical cell for measurements.

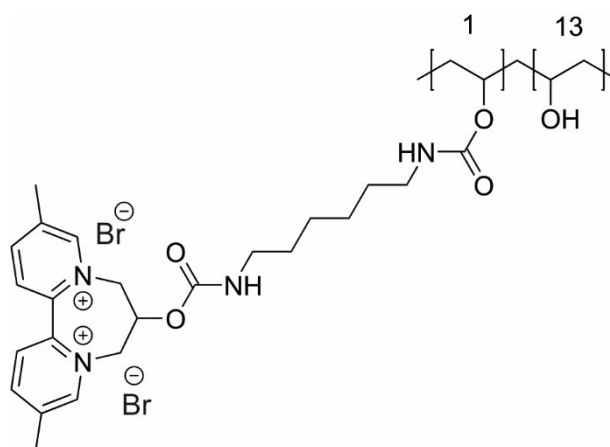
### **1.4 Electrochemistry**

Mediated electron transfer electrochemical measurements were performed under ambient lab conditions. The direct electron transfer experiment as well as the control experiments in Figure S1 were performed in a glovebox filled with N<sub>2</sub> (MBraun). All electrochemical experiments were recorded on a Gamry Reference 600™ potentiostat. A rotating disk glassy carbon working electrode with a diameter of 3 or 5 mm was used in a three-electrode setup. Ag/AgCl 3M KCl was used as reference electrode and Pt wire as counter electrode. Commercial Tris base (Sigma Aldrich), citric acid (Sigma Aldrich) and KI (Fluka Analytics) were used to prepare the electrolyte containing Tris-citrate buffer (50 mM, pH 8.8) and KI (0.1 M).

### **1.5 Spectroelectrochemistry**

FTIR spectroelectrochemical titrations were performed using a homebuilt transition mode electrochemical cell based on a design by Moss and coworkers.<sup>4</sup> A 50  $\mu$ m thick gold mesh was used as a working electrode, deposited on a CaF<sub>2</sub> window. A mixture of 22  $\mu$ L of 1.78 mM sulfide-protected

*DdHydAB* and 63.3  $\mu\text{L}$  of 15.8  $\text{mg mL}^{-1}$  redox polymer P1 was prepared. 80  $\mu\text{L}$  of this mixture was deposited on the gold mesh in 20  $\mu\text{L}$  portions and allowed to dry for 1 h after each addition at room temperature. The window was then fixed into the electrochemical cell and 40  $\mu\text{L}$  of Tris-citrate buffer (50 mM pH 8.8) with KI (0.1 M) was pipetted over the film. A platinum counter electrode and a Ag/AgCl (sat. KCl) reference electrode completed the three-electrode system. The reference electrode was calibrated before and after each measurement using (hydroxymethyl)ferrocene (Aldrich, +420 mV vs SHE) as a reference, to ensure the potential stability during the course of the experiment. The potential was controlled by an Autolab PGSTAT101 potentiostat using Nova software. Each potential was applied for 30 minutes prior to measuring IR spectra, in order to obtain equilibrium. All potentials referred to in the text are quoted versus the standard hydrogen electrode (SHE). The temperature of the cell was maintained at 10  $^{\circ}\text{C}$  using a water circulator system (Huber, Offenburg). Spectra were measured on a Bruker IFS 66v/S FTIR spectrometer equipped with a nitrogen cooled Bruker mercury cadmium telluride (MCT) detector. Spectra were collected in the double-sided, forward-backward mode with a resolution of 2  $\text{cm}^{-1}$ , an aperture setting of 2.5 mm and a scan velocity of 20 KHz. Spectra are the average of 1000 scans. Data were processed using home-written routines in the MATLAB<sup>TM</sup> environment.



**Scheme S1.** Structure of the redox polymer P1

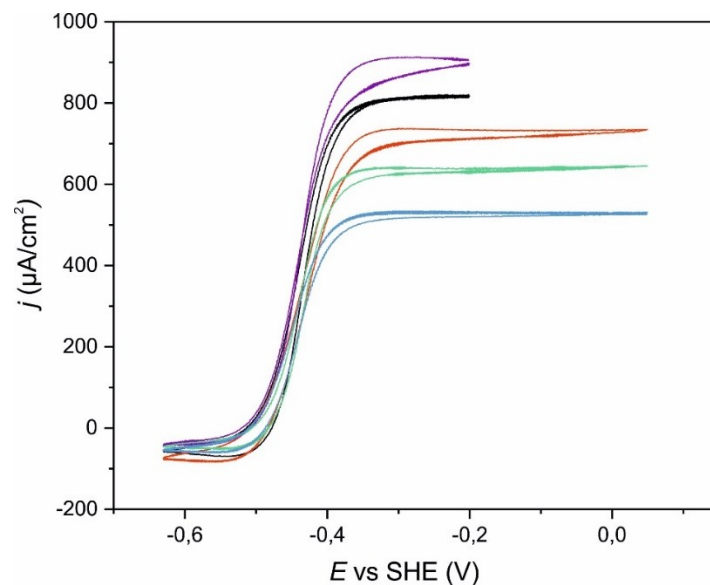


**Figure S1.** Cyclic voltammetry experiments of five different GCEs modified with protected *DdHydAB* embedded in the redox polymer P1. Conditions: Tris-citrate buffer (50 mM, pH 8.8) with KI (100 mM), 2000 rpm, 20 mV s<sup>-1</sup>, room temperature.

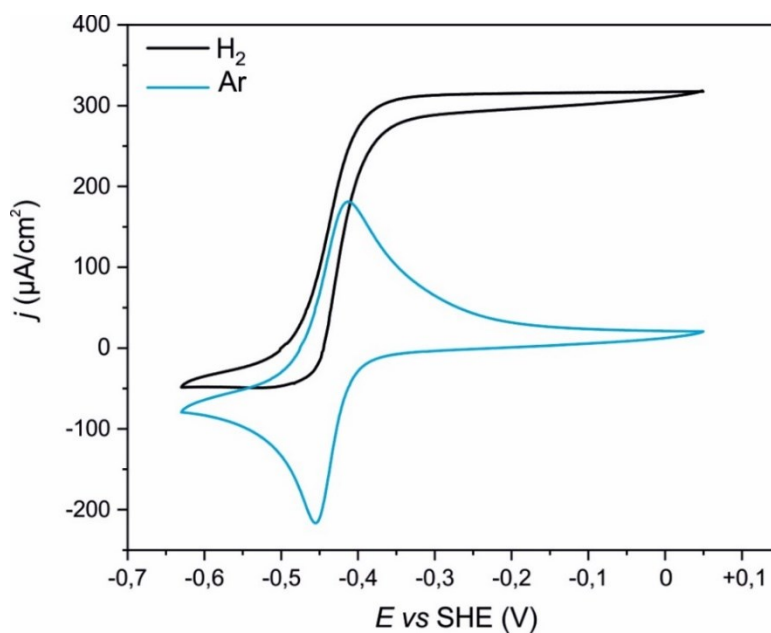


**Figure S2.** Cyclic voltammetry experiments under Ar (blue trace) and under H<sub>2</sub> (black trace) of unprotected *DdHydAB* embedded in the redox polymer P1. The electrode was prepared and measured in an anaerobic glovebox. Conditions: 50 mM Tris-citrate buffer pH 8.8 with 100 mM KI, 2000 rpm, 20 mV s<sup>-1</sup>, room temperature.

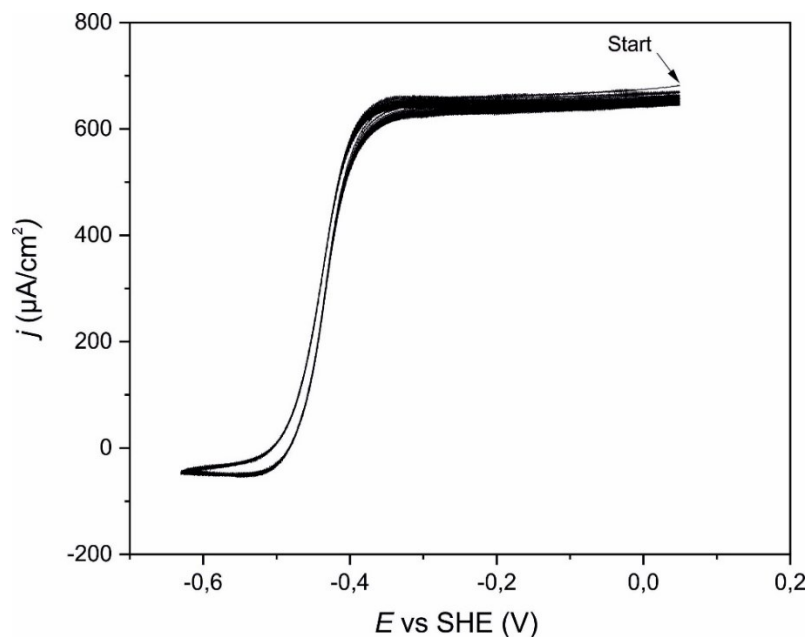


**Figure S3.** Successive cyclic voltammetry scans (15 scans) of protected *DdHydAB* embedded in the redox polymer P1 under hydrogen. Scanning was started from positive potentials. Conditions: Tris-citrate buffer (50 mM, pH 8.8) with KI (100 mM), 2000 rpm, 20 mV s<sup>-1</sup>, room temperature.

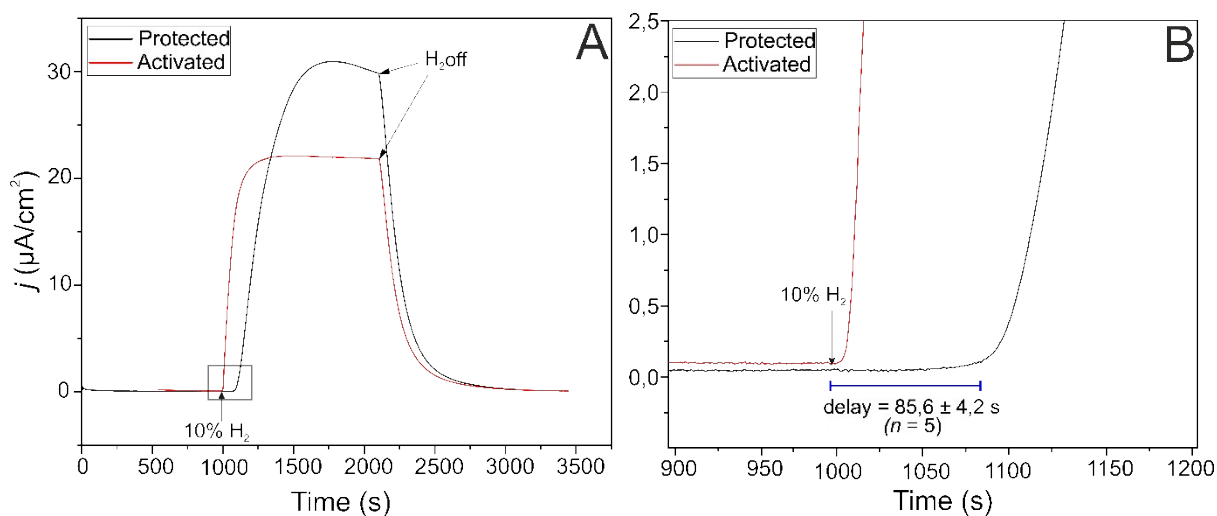


**Figure S4.** Chronoamperometry experiments of protected *DdHydAB* embedded in redox polymer before (black) and after (red) activation. A potential of +199 mV vs SHE was applied under Ar. After the current stabilized close to 0, 10% H<sub>2</sub> was added to the gas flow then switched off again upon reaching maximum current (indicated by arrows) (A). Zoom-in view of H<sub>2</sub> addition section (B). Conditions: Tris-citrate buffer (50 mM, pH 8.8) with KI (100 mM), 2000 rpm, room temperature.

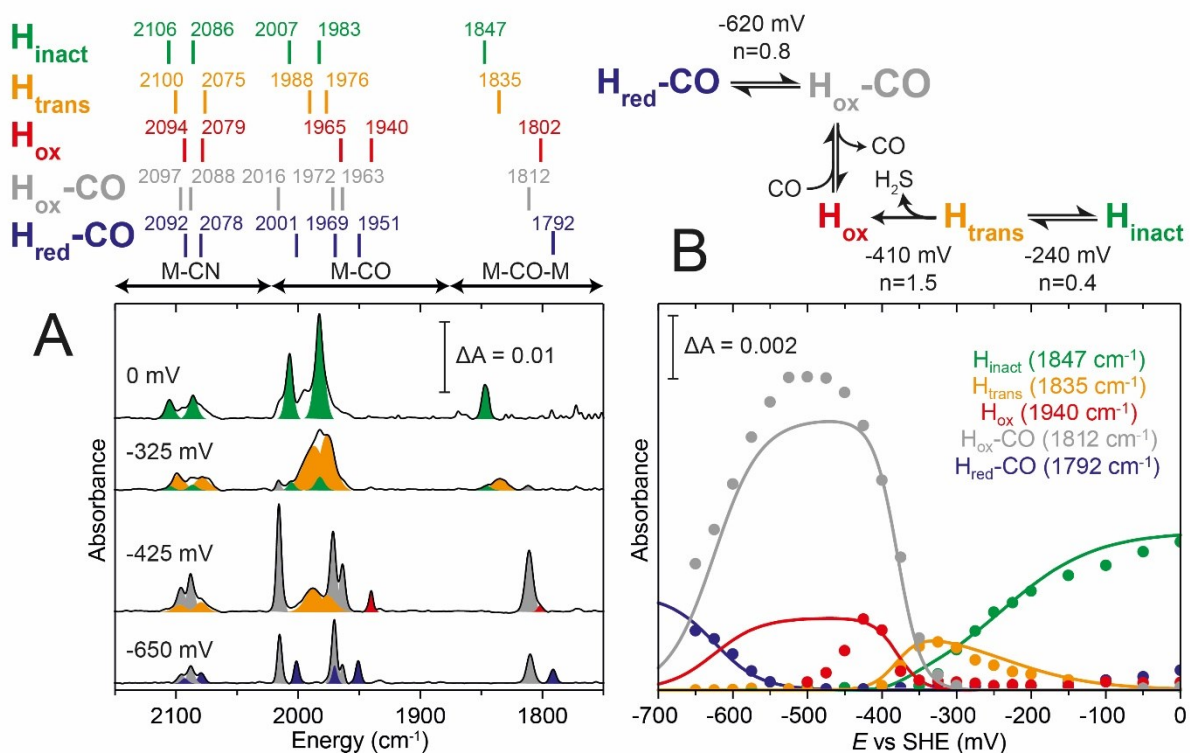


**Figure S5.** FTIR spectroelectrochemistry of reactivation of sulfide-protected *DdHydAB* in a redox polymer hydrogel matrix. A) FTIR spectra of *DdHydAB* at various applied potentials during the redox titration, highlighting the main species observed: H<sub>inact</sub> (green peaks), H<sub>trans</sub> (orange peaks), H<sub>ox</sub> (red peaks), H<sub>ox</sub>-CO (gray peaks), H<sub>red</sub>-CO (purple peaks). B) The intensities of the bridging CO band (between 1820 cm<sup>-1</sup> and 1790 cm<sup>-1</sup>) for the H<sub>inact</sub> (green circles, 1847 cm<sup>-1</sup>), H<sub>trans</sub> (orange circles, 1835 cm<sup>-1</sup>), H<sub>ox</sub>-CO (gray circles, 1812 cm<sup>-1</sup>), and H<sub>red</sub>-CO (purple circles, 1792 cm<sup>-1</sup>), and the terminal CO band from the H<sub>ox</sub> state (red circles, 1940 cm<sup>-1</sup>) are plotted against the applied potential. The data were fitted with curves based on the Nernst equation, and the scheme above the figure shows the *E* and *n* values used for fitting. The sample preparation is described in the supplementary methods. Measurements were carried out at 10 °C, and with 2 cm<sup>-1</sup> resolution. The applied potential was swept from positive to negative.

Due to the overlap on the most intense bands of H<sub>inact</sub>, H<sub>trans</sub>, H<sub>ox</sub>-CO and H<sub>red</sub>-CO (between 2020 cm<sup>-1</sup> and 1950 cm<sup>-1</sup>), which convolutes the analysis, we chose to follow the intensities of the more well-separated bridging CO bands (between 1850 cm<sup>-1</sup> and 1790 cm<sup>-1</sup>). However, the most intense band for H<sub>ox</sub> (1940 cm<sup>-1</sup>) is well separated from all the other peaks of the various states, and so the intensity of this peak was followed for the H<sub>ox</sub> state. It was previously reported for the enzyme in solution in the presence of soluble redox mediators, that the H<sub>inact</sub> state converts to the H<sub>trans</sub> state at -140 mV vs SHE with *n* = 1.<sup>3</sup> For the enzyme embedded in a redox polymer (Figure S5), the conversion of the H<sub>inact</sub> state to the H<sub>trans</sub> state occurs with a lower midpoint potential (-240 mV) and *n* = 0.4 behavior. This can be explained in part by the higher pH (8.8 vs 8) used in the current redox titration compared with that performed with the enzyme in solution. All the potentials are pH dependent and accordingly

shifted to more negative values for pH 8.8 compared with pH 8. Electron transfer rates through the polymer are likely to be extremely poor at applied potentials much more positive than the redox midpoint potential of the viologen moieties in the polymer (-440 mV). This further explains the more negative midpoint potential of the  $H_{\text{inact}}$  to  $H_{\text{trans}}$  transition, as well as the  $n = 0.4$  behavior. In the solution measurements, soluble mediators including anthraquinone-1,5-disulfonic acid ( $E_{\text{m},7} = -234$  mV) and anthraquinone-2-sulfonate ( $E_{\text{m},7} = -277$  mV) were used to facilitate rapid electron exchange between the working electrode and the enzyme.

As the applied potential approaches that of the viologen potential, the conversion of  $H_{\text{inact}}$  to  $H_{\text{trans}}$  goes to completion and shortly afterwards the  $H_{\text{trans}}$  state is converted to a mixture of  $H_{\text{ox}}$  and  $H_{\text{ox}}\text{-CO}$ , with a midpoint potential of -410 mV and  $n = 1.5$ . Presumably, at this point the active sites of some enzyme molecules have degraded involving the release of the CO ligands, which then bind to the activated enzymes in the  $H_{\text{ox}}$  state.<sup>5</sup> It does not require much of the enzyme to be damaged to inhibit a large number of the active enzymes because *i)* each active site contains three CO ligands, *ii)* *DdHydAB* has a high affinity for CO<sup>6</sup>, and *iii)* the small volume of the spectroelectrochemical cell enables accumulation of CO. Other than this, the behaviour is similar to that reported for the solution measurements, but with a slightly more negative potential, reflecting the higher pH in the current experiments. The high value of  $n$  reflects the fact that this step is irreversible: there is no  $\text{H}_2\text{S}$  in solution available to rebind the active site, so the reaction proceeds to completion in a kinetic fashion, where the kinetics depend on the applied potential. Interestingly, below the redox midpoint potential of the polymer, at around the potential that  $H_{\text{ox}}$  should be converted to the  $H_{\text{red}}/H_{\text{red}}\text{H}^+$  states, the  $H_{\text{ox}}$  state is lost completely and replaced by an increase in the  $H_{\text{ox}}\text{-CO}$  state. As this step cannot not involve a simple one-electron reduction of the enzyme, it cannot be fit with the Nernst equation.

Finally, at very low potential (-620 V vs SHE) the  $H_{\text{ox}}\text{-CO}$  state is converted to the  $H_{\text{red}}\text{-CO}$  state, with a potential slightly more negative than that previously reported at pH 8.<sup>7</sup> Overall, the spectroelectrochemistry experiments demonstrate that the behaviour of the enzyme in the redox polymer is similar to the behaviour in solution, and that the reactivation of the enzyme follows the same pathway. The main difference, the formation of a large amount of the  $H_{\text{ox}}\text{-CO}$  state observed in the spectroelectrochemical cell, is unlikely to occur in the electrochemical experiments during purging of the electrochemical cell with  $\text{H}_2$ .

## References

- 1 S. Hardt, S. Stapf, J. A. Birrell, O. Rüdiger, V. Fourmond, C. Léger, N. Plumeré, Reversible H<sub>2</sub> oxidation and evolution by hydrogenase embedded in a redox polymer film, submitted March 2020.
- 2 J. A. Birrell, K. Wrede, K. Pawlak, P. Rodriguez-Maciá, O. Rüdiger, E. J. Reijerse and W. Lubitz, *Isr. J. Chem.*, 2016, **56**, 852–863.
- 3 P. Rodríguez-Maciá, E. J. Reijerse, M. van Gastel, S. DeBeer, W. Lubitz, O. Rüdiger and J. A. Birrell, *J. Am. Chem. Soc.*, 2018, **140**, 9346–9350.
- 4 D. Moss, E. Nbedryk, J. Breton and W. Mantele, *Eur. J. Biochem.*, 1990, **187**, 565–572.
- 5 a) S. P. J. Albracht, W. Roseboom and E. C. Hatchikian, *J Biol Inorg Chem*, 2006, **11**, 88–101; b) P. Rodríguez-Maciá, J. A. Birrell, W. Lubitz and O. Rüdiger, *Chempluschem*, 2017, **82**, 540–545;
- 6 A. Parkin, C. Cavazza, J. C. Fontecilla-Camps and F. A. Armstrong, *J. Am. Chem. Soc.*, 2006, **128**, 16808–16815.
- 7 a) P. Rodríguez-Maciá, K. Pawlak, O. Rüdiger, E. J. Reijerse, W. Lubitz and J. A. Birrell, *J. Am. Chem. Soc.*, 2017, **139**, 15122–15134; b) P. Rodríguez-Maciá, E. Reijerse, W. Lubitz, J. A. Birrell and O. Rüdiger, *J. Phys. Chem. Lett.*, 2017, **8**, 3834–3839.